LIND, M. D. & CHRISTE, K. O. (1972). *Inorg. Chem.* **11**, 608-612.
MITCHELL, S. J. & HOLLOWAY, J. H. (1971). *J. Chem. Soc. A*, S. 2789-2794.
MORRELL, B. K., ZALKIN, A., TRESSAUD, A. & BARTLETT, N. (1973). *Inorg. Chem.* **12**, 2640-2644.
MÜLLER, U. (1978). *Acta Cryst.* A**34**, 256-267.
MÜLLER, U. (1979*a*). *Acta Cryst.* A**35**, 188-193.
MÜLLER, U. (1979*b*). *Z. Anorg. Allg. Chem.* **454**, 75-81.
MÜLLER, U. (1981). *Acta Cryst.* B**37**, 532-545.
MÜLLER, U. (1984). *Acta Cryst.* C**40**, 915-917.
MÜLLER, U. (1985). *Z. Kristallogr.* **170**, 135-137.
PREISS, H. (1966*a*). *Z. Anorg. Allg. Chem.* **346**, 272-278.
PREISS, H. (1966*b*). *Z. Chem.* **6**, 350-351.
PREISS, H. (1968). *Z. Anorg. Allg. Chem.* **362**, 13-18.
SCHWARZ, W. & GUDER, H. J. (1978). *Z. Anorg. Allg. Chem.* **444**, 105-111.
ZACHARIASEN, W. H. (1949). *Acta Cryst.* **2**, 296-298.

Acta Cryst. (1986). B**42**, 564-575

Neutron Low-Temperature (4 and 20 K) and X-ray High-Pressure ($6{\cdot}5\times10^2$ and $9{\cdot}8\times10^2$ MPa) Structures of the Organic Superconductor Di(2,3,6,7-tetramethyl-1,4,5,8-tetraselenafulvalenium) Hexafluorophosphate,* $(TMTSF)_2PF_6$

BY BERNARD GALLOIS, JACQUES GAULTIER, CHRISTIAN HAUW AND TAJ-DINE LAMCHARFI

Laboratoire de Cristallographie et de Physique Cristalline, LA-CNRS 144, *Université de Bordeaux* I, 33405 *Talence, France*

AND ALAIN FILHOL

Institut Laue-Langevin, 156*X*, 38042 *Grenoble CEDEX, France*

(*Received* 30 *August* 1985; *accepted* 15 *April* 1986)

Abstract

The Bechgaard salts $(TMTSF)_2X$ (with X a small centro- or non-centrosymmetric anion) show several kinds of ground states, in particular a superconducting one at low temperatures ($T<1{\cdot}5$ K), under a pressure which is strongly dependent on the nature of the anion X. Since intrachain and interchain interactions and anion disorder are key parameters in the understanding of this behaviour, single-crystal structures are presented of $(TMTSF)_2PF_6$ $[2(C_{10}H_{12}Se_4)^{1/2+}.PF_6^-,\ M_r=1041{\cdot}06]$ at low temperatures (4 and 20 K) or under high pressures ($6{\cdot}5\times10^2$ and $9{\cdot}8\times10^2$ MPa) as well as thermal expansion (4 to 295 K) and isothermal compressibility data (10^{-1} to 16×10^2 MPa). The main structure-determination components are: neutron structures at ambient pressure: $\lambda=1{\cdot}5001(8)$ Å, space group $P\bar{1}$ with $Z=1$, $\mu_{(300\,K)}\sim0{\cdot}17$ mm^{-1}; at 20 K: $a=7{\cdot}067\,(4)$, $b=7{\cdot}636\,(2)$, $c=13{\cdot}319\,(4)$ Å, $\alpha=84{\cdot}11\,(3)$, $\beta=88{\cdot}06\,(3)$, $\gamma=70{\cdot}10\,(3)°$, $V=672{\cdot}26$ Å^3, $D_x=2{\cdot}571$ Mg m^{-3}, $R=wR=0{\cdot}082$ for 1249 reflections; at 4 K: $a=7{\cdot}077\,(2)$, $b=7{\cdot}632\,(1)$, $c=13{\cdot}322\,(2)$ Å, $\alpha=84{\cdot}14\,(2)$, $\beta=88{\cdot}00\,(2)$, $\gamma=70{\cdot}15\,(2)°$, $V=673{\cdot}25$ Å^3, $D_x=2{\cdot}568$ Mg m^{-3}, $R=wR=0{\cdot}078$ for 1176 reflections. X-ray (Mo $K\alpha$) structures at room temperature; space group $P\bar{1}$ with $Z=1$, $\mu_{(300\,K)}=10{\cdot}267$ mm^{-1}; for $P=6{\cdot}5\times10^2$ MPa; $a=7{\cdot}135\,(7)$, $b=7{\cdot}598\,(7)$, $c=13{\cdot}325\,(10)$ Å, $\alpha=83{\cdot}64\,(8)$, $\beta=87{\cdot}03\,(8)$, $\gamma=70{\cdot}52\,(8)°$, $V=676{\cdot}74$ Å^3, $D_x=2{\cdot}554$ Mg m^{-3}, $R=wR=0{\cdot}048$ for 1958 reflections; for $P=9{\cdot}8\times10^2$ MPa: $a=7{\cdot}020\,(7)$, $b=7{\cdot}536\,(7)$, $c=13{\cdot}216\,(10)$ Å, $\alpha=83{\cdot}77\,(8)$, $\beta=87{\cdot}53\,(8)$, $\gamma=70{\cdot}19\,(8)°$, $V=653{\cdot}89$ Å^3, $D_x=2{\cdot}644$ Mg m^{-3}, $R=wR=0{\cdot}067$ for 1264 reflections. The set of high-pressure structural data is one of the first ever obtained for a Bechgaard salt. These results together with the (295 K, 10^{-1} MPa) data in the literature allow a detailed description of the crystal-packing evolution under constraint. Interplanar Se...Se distances are the only TMTSF intrastack parameters strongly T or P dependent. Both temperature and pressure lead to a shortening of TMTSF intra- and interstack distances in the ratio 1:1·5. The ordering of the PF_6 anion is also described.

Introduction

Since the first observation by Jérome, Mazaud, Ribault & Bechgaard (1980) of superconductivity in $(TMTSF)_2X$ salts (TMTSF = tetramethyltetraselenafulvalene; X^- = small anion such as PF_6^-, AsF_6^-, ClO_4^-, ReO_4^-, NO_3^- *etc.*), the physical properties of these compounds have been the subject of extensive studies over a wide temperature and/or pressure range [for a review see *e.g.* Jérome & Schulz (1982)]. $(TMTSF)_2X$ salts are quasi-one-dimensional (1D)

* Recommended IUPAC name: di(4, 4', 5, 5'-tetramethyl-$\Delta^{2,2'}$-bi-1,3-diselenolyliden)ium hexafluorophosphate.

0108-7681/86/060564-12$01.50

metals at room temperature and ambient pressure which generally exhibit an insulating magnetic or non-magnetic low-temperature ground state. Pressure is then needed to suppress the 'metal-to-insulator' phase transition and possibly to reach the superconducting ground state. Thus, both pressure and temperature are important parameters in the study of these compounds.

The role of competing instabilities leading to one of the possible ground states under given temperature and pressure (T, P) conditions is not yet clear. The interplay of driving forces is at present mostly understood through theoretical models in which some major parameters are structural ones. For example, since electrical conduction occurs mainly *via* the overlap of the selenium orbitals, the electronic transport properties will be clearly influenced by T- and/or P-induced changes in the selenium network. Special interest is thus devoted by physicists to the Se···Se intra- and intermolecular interactions, the former being related to the electron scattering along the TMTSF columns while the latter mainly influence the electronic dimensionality.

However, structural data on $(TMTSF)_2X$ compounds under constraint are scarce and the above models often rely on room-temperature and ambient-pressure data only. More precisely, to our knowledge the only high-pressure structure already published is for $(TMTSF)_2AsF_6$ at $26{\cdot}5\times10^2$ MPa (Finger, Beno, Williams & Hazen, 1984). In the literature, structures at low enough temperatures are mainly devoted to salts with non-centrosymmetric anions, *e.g.* $X^-=ReO_4^-$ (Moret, Pouget, Comès & Bechgaard, 1982; Rindorf, Soling & Thorup, 1984); $X^-=ClO_4^-$ (Gallois, Chasseau, Gaultier, Hauw, Filhol & Bechgaard, 1983; Gallois, Meresse, Gaultier & Moret, 1985); $X^-=BF_4^-$ (Emge, Williams, Leung, Schultz, Beno & Wang, 1985).

In these salts the anions are known to order in two quite distinct orientations which may influence the organic lattice packing. However, although $(TMTSF)_2X$ salts are isostructural with very similar lattice parameters at room temperature, our knowledge of the latter type of organic distortion may not be generalized to the case where X^- is a centrosymmetric anion.

The aim of the present paper is thus to improve our understanding of the mechanisms driving the various observed instabilities in $(TMTSF)_2X$ by studying the influence of T or P on the structure of a Bechgaard salt with a centrosymmetric anion [namely $(TMTSF)_2PF_6$]. The latter compound undergoes a 'metal-to-insulator' phase transition at $T_{MI}\simeq 11{\cdot}5$ K (Bechgaard, Jacobsen, Mortensen, Pedersen & Thorup, 1980), the ground state of which is antiferromagnetic as indicated by magnetic measurements (Torrance, Pedersen & Bechgaard, 1982). Above $9{\cdot}5\times10^2$ MPa, the metal–insulator instability is suppressed and superconductivity occurs at $T_c\simeq 1{\cdot}2$ K (Jérome, Mazaud, Ribault & Bechgaard, 1980). The corresponding T, P phase diagram may be found, for example, in Jérome & Schulz (1982).

The room-temperature structure of $(TMTSF)_2PF_6$ has already been investigated in detail by Thorup, Rindorf, Soling & Bechgaard (1981). The TMTSF units are nearly planar and stacked along the a cell axis. Within a column, TMTSF units repeat by inversion leading to zig-zag type stacking. The column is thus slightly dimerized as indicated by the values of the two independent intrastack distances ($d_1=3{\cdot}66$; $d_2=3{\cdot}63$ Å). The TMTSF columns form ab sheets spaced by anions. As regards interatomic distances only, two magnitudes of interchain Se···Se coupling are observed (a short 3·879 Å on the one hand and three longer distances of 3·934, 3·934 and 3·959 Å on the other). The inorganic anions PF_6^- are located at the inversion centre of the unit cell and are surrounded by TMTSF methyl groups. They appear to be statistically disordered.

In the following we discuss $(TMTSF)_2PF_6$ structures at two low temperatures (above and below T_{MI}) under normal pressure and at room temperature under two high pressures. This allows us to compare the temperature and pressure effects on the crystal packing. In addition, the joint effect of T and P will be discussed in a separate paper (Gallois, Gaultier, Filhol & Vettier, 1986) on the 1·7 K, 7×10^2 MPa structure of $(TMTSF)_2PF_6$ as determined by neutron diffraction.

Experimental

(i) *Low temperature*

The low-temperature measurements were performed at the Institut Laue-Langevin (Grenoble, France) on the single-crystal 4-circle diffractometer $D10$ installed at a thermal neutron guide of the High Flux Reactor. The main experimental conditions were the following: incoming beam wavelength = 1·5001 (8) Å, neutron flux at sample position $\sim 5\times10^6$ neutrons $cm^{-2}\,s^{-1}$, low temperatures achieved with a continuous He-gas-flow cryostat (Zeyen, Chagnon, Disdier & Morin, 1984).

The sample was a (non-deuterated) twinned single crystal $2{\cdot}9\times0{\cdot}3\times0{\cdot}5$ mm. The geometry of the twinning is such that twins I and II have the same a cell axis. The reciprocal axes b_I^* and b_{II}^* on the one hand and c_I^* and c_{II}^* on the other are parallel but in opposite directions. The b^*c^* planes of both lattices are thus superimposed. In the measured part of the reciprocal space, the $(hkl)_I$ and $(hkl)_{II}$ reflections do not overlap except if $h=0$. The volume of the twins was in the ratio 0·6:0·4.

Lattice parameters of $(TMTSF)_2PF_6$ at 20 temperatures in the range 3·9 to 295 K were obtained by a least-squares refinement of the angular positions of

13 to 17 strong centred reflections (Fig. 1).* The intensities of 1249 and 1176 independent Bragg reflections ($\sin\theta/\lambda < 0{\cdot}4714$ Å^{-1}; range of h: 0 to 6, k: −7 to 7 and l: −12 to 12) were collected at 4 and 20 K respectively, by ω scans of 31 steps and with the angular width an experimental function of the Bragg angle θ. The data reduction was performed with the $\sigma(I)/I$ algorithm of Lehmann & Larsen (1974). The intensities were corrected for the Lorentz factor to obtain structure factors (F_o) but no absorption correction was made [$\mu_{(300\,K)}$ calculated = 1·799, $\mu_{(300\,K)}$ measured = 1·71 cm^{-1}].

The least-squares refinement of both structures was of the block-diagonal type based on F_o (all measured reflections included) with the X-ray room-temperature atomic coordinates as starting values (Thorup *et al.*, 1981). Atomic scattering factors were from *International Tables for X-ray Crystallography* (1974). The intensities being very weak, unit weights were found to be reasonably adequate here. The atomic thermal parameters, being very small at 20 and 4 K,* were only refined isotropically. The final value of the reliability factor $R = \sum||F_o|-|F_c||/\sum|F_o|$ is $R \simeq 0{\cdot}082$ and $R \simeq 0{\cdot}078$ for the 20 and 4 K structures respectively. Atomic coordinates are given in Table 1, bond lengths and angles are displayed in Fig. 2.

(ii) *High pressure*

The high-pressure diffraction measurements were performed with a gasketed diamond-anvil cell designed by Ahsbahs (1984) and mounted on a single-crystal X-ray diffractometer. The pressure-transmitting medium was water up to 7×10^2 MPa and Fluorinert FC75† (C_8F_{18}) above since the freezing pressure of water is about 1 GPa (Bridgmann, 1911). The pressure in the cell was measured from the shift ($d\lambda/dP = 42{\cdot}6\times10^{-2}$ Å MPa^{-1}) of the optical absorption maximum ($\lambda_0 = 5270$ Å at 0·1 MPa) of nickel(dimethylglyoxime)$_2$ with an estimated accuracy of ~50 MPa (Davies, 1968) up to 36×10^2 MPa (Loumrhari, 1983). Owing to size limitations inherent in the pressure cell, the dimensions of the samples were less than $0{\cdot}15\times0{\cdot}1\times0{\cdot}1$ mm. The crystals all showed the kind of twinning described above.

The cell parameters at six pressures in the range 0·1 to 16×10^2 MPa were obtained from the observed angular positions of centred reflections (Fig. 3).*

* A table of the cell dimensions of $(TMTSF)_2PF_6$ in the temperature range 4 to 295 K (0.1 MPa) and in the pressure range 0.1 to 16×10^2 MPa (295 K) as well as lists of structure factors corresponding to the 4, 20 K, $6{\cdot}5\times10^2$ and $9{\cdot}8\times10^2$ MPa structures reported here have been deposited with the British Library Document Supply Centre as Supplementary Publication No. SUP 42953 (39 pp.). Copies may be obtained through The Executive Secretary, International Union of Crystallography, 5 Abbey Square, Chester CH1 2HU, England.

* See deposition footnote.

† 'Fluorinert' is a trademark of the 3M Company.

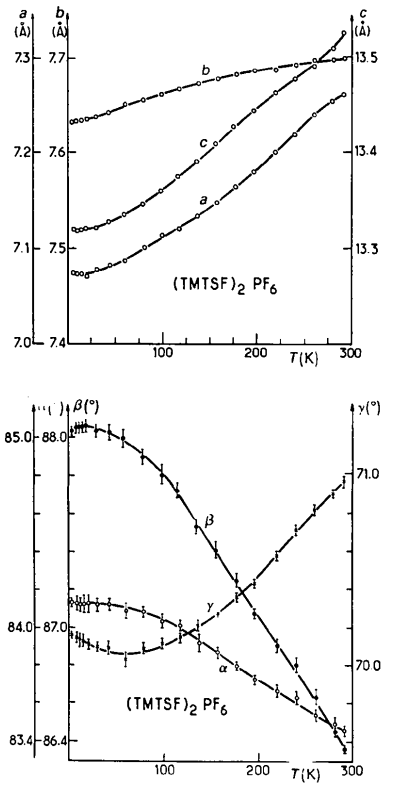

Fig. 1. Cell parameters as a function of temperature.

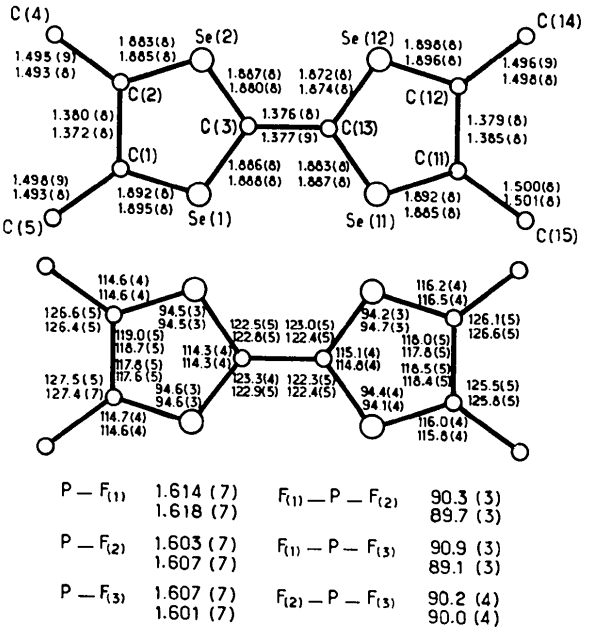

Fig. 2. Bond lengths (Å) and angles (°) for $(TMTSF)_2PF_6$ structures at 20 and 4 K under normal pressure. For each quantity the 4 K value is displayed below the 20 K one. E.s.d.'s are given in parentheses.

The $6{\cdot}5\times10^2$ MPa Bragg intensities were recorded on a Stoe diffractometer (lifting counter technique; equi-inclination geometry). In this case a direct-cell axis of the crystal must be set parallel to the instrument axis; this was obtained with the help of a preliminary crystal alignment by means of X-ray photographic methods. 1958 independent intensities were collected (ω scans, Mo $K\alpha$ radiation) up to $\sin\theta/\lambda = 0{\cdot}597$ Å^{-1} within the range h, k and l: 0 to 8, −7 to 7 and −16 to 16 respectively.

The $9{\cdot}8\times10^2$ MPa Bragg intensities were recorded on a Siemens AED 4-circle diffractometer since the initial crystal orientation in the pressure cell changes too much under such a constraint to allow for easy setting on the Stoe diffractometer. 1264 independent reflections were measured (ω scans, Mo $K\alpha$ radiation) up to $\sin\theta/\lambda = 0{\cdot}597$ Å^{-1} within the range h, k and l: 0 to 3, −8 to 8 and −15 to 15 respectively.

The pressure-cell geometry introduces blind spots (steel pillars shadowing the incident or diffracted beam), and furthermore beryllium and diamond parasitic scattering and/or diffraction lines induce a high and inhomogeneous background. For the data reduction, we have used a reflection-by-reflection display of line profiles on a computer graphics screen together with interactive facilities for the rejection of bad profiles and the adjustment of background levels on

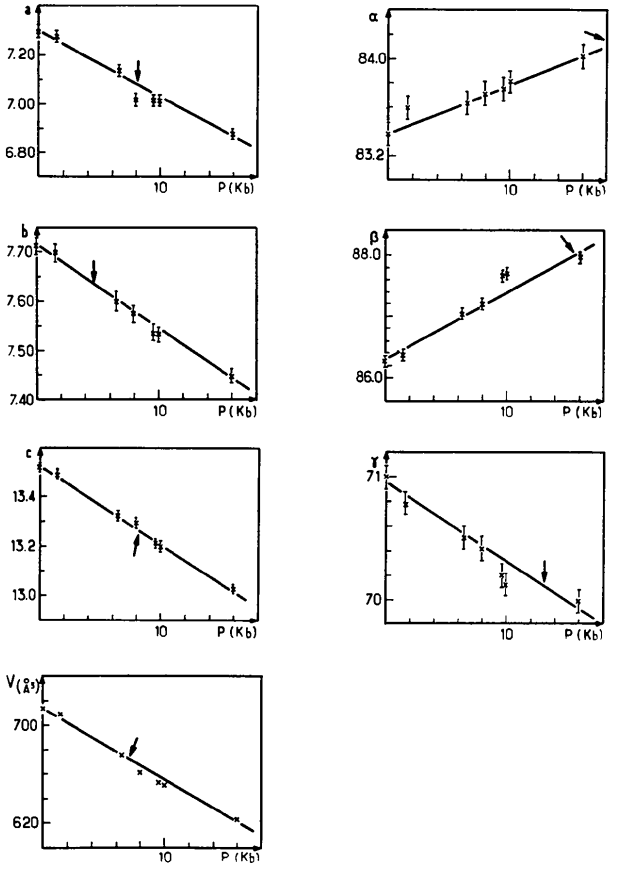

Fig. 3. Cell parameters as a function of pressure. For comparison, the arrows indicate the value of the lattice parameter at 4 K at room pressure.

Table 1. *Fractional coordinates (x, y, z) and isotropic thermal parameters (B) of atoms at 20 and 4 K under normal pressure*

For each atom the 20 and 4 K values are given on successive lines. Fractional coordinates are $\times10^3$ for H atoms and $\times10^4$ for others. E.s.d.'s are given in parentheses.

The corresponding cell dimensions a, b, c (Å), α, β, γ (°) are: 7·067 (4), 7·636 (2), 13·319 (4), 84·11 (3), 88·06 (3), 70·10 (3) at 20 K; 7·077 (2), 7·632 (1), 13·322 (2), 84·14 (2), 88·00 (2), 70·15 (2) at 4 K.

	x	y	z	B (Å^2)
Se(1)	3069 (7)	3349 (6)	6167 (3)	0·62
	3068 (7)	3351 (5)	6162 (3)	0·55
Se(2)	1622 (7)	7503 (6)	5118 (3)	0·52
	1624 (7)	7502 (6)	5116 (3)	0·49
Se(11)	3742 (7)	1690 (6)	3846 (3)	0·42
	3747 (7)	1682 (6)	3845 (3)	0·46
Se(12)	2213 (7)	5841 (6)	2807 (3)	0·71
	2203 (7)	5851 (5)	2807 (3)	0·56
P	0	0	0	0·26
	0	0	0	0·20
F(1)	152 (9)	−1226 (8)	1075 (4)	0·53
	156 (10)	−1234 (8)	1076 (4)	0·50
F(2)	2358 (9)	−1011 (8)	−183 (4)	0·81
	2362 (10)	−1006 (8)	−183 (4)	0·71
F(3)	466 (9)	1611 (8)	527 (4)	0·63
	461 (10)	1605 (8)	527 (4)	0·57
C(1)	2329 (8)	5338 (7)	7001 (4)	0·43
	2342 (8)	5343 (6)	6999 (3)	0·39
C(2)	1694 (8)	7143 (7)	6538 (4)	0·51
	1699 (9)	7136 (6)	6537 (3)	0·40
C(3)	2537 (8)	4925 (7)	4948 (4)	0·42
	2525 (8)	4933 (7)	4944 (4)	0·36
C(4)	1026 (8)	8907 (7)	7050 (4)	0·62
	1039 (9)	8896 (7)	7049 (4)	0·40
C(5)	2493 (8)	4739 (7)	8110 (4)	0·73
	2490 (9)	4746 (7)	8104 (4)	0·52
C(11)	3730 (8)	2052 (7)	2420 (4)	0·50
	3723 (8)	2051 (6)	2424 (4)	0·35
C(12)	3067 (8)	3859 (7)	1962 (4)	0·57
	3064 (8)	3866 (6)	1966 (3)	0·35
C(13)	2790 (8)	4265 (7)	4012 (4)	0·33
	2810 (9)	4264 (7)	4009 (3)	0·30
C(14)	2938 (8)	4421 (7)	850 (4)	0·45
	2948 (9)	4412 (7)	852 (4)	0·30
C(15)	4456 (8)	306 (7)	1886 (4)	0·42
	4462 (9)	311 (7)	1884 (3)	0·30
H(101)	−53 (2)	958 (2)	699 (1)	2·09
	−57 (2)	960 (2)	698 (1)	1·93
H(102)	607 (2)	−38 (2)	198 (1)	2·22
	608 (2)	−38 (2)	197 (1)	2·16
H(103)	196 (2)	597 (2)	854 (1)	1·89
	197 (2)	598 (1)	855 (1)	1·45
H(111)	159 (2)	387 (2)	829 (1)	1·55
	157 (3)	385 (1)	832 (1)	1·60
H(112)	400 (2)	395 (2)	831 (1)	2·10
	403 (2)	394 (2)	832 (1)	1·99
H(113)	133 (2)	861 (2)	787 (1)	2·48
	133 (2)	863 (2)	787 (1)	2·17
H(121)	173 (2)	987 (2)	673 (1)	1·91
	174 (2)	987 (1)	673 (1)	1·74
H(122)	145 (2)	475 (2)	59 (1)	3·08
	142 (2)	475 (2)	58 (1)	2·94
H(123)	333 (2)	561 (2)	66 (1)	2·32
	336 (2)	561 (2)	66 (1)	2·36
H(131)	384 (2)	330 (2)	43 (1)	2·95
	386 (2)	330 (2)	44 (1)	2·59
H(132)	421 (2)	59 (2)	109 (1)	2·08
	417 (2)	59 (2)	108 (1)	1·99
H(133)	376 (2)	−66 (2)	218 (1)	2·22
	375 (2)	−69 (2)	219 (1)	2·10

Table 2. *Fractional coordinates (x, y, z) and isotropic thermal parameters (B/B_{eq}) of atoms under $6{\cdot}5\times10^2$ and $9{\cdot}8\times10^2$ MPa at 295 K*

For each atom the $6{\cdot}5\times10^2$ and the $9{\cdot}8\times10^2$ MPa values are given on successive lines. Fractional coordinates are $\times10^4$. E.s.d.'s are given in parentheses.

The corresponding cell dimensions *a*, *b*, *c* (Å), α, β, γ (°) are: 7·135 (7), 7·598 (7), 13·325 (10), 83·64 (8), 87·03 (8), 70·52 (8) at $6{\cdot}5\times10^2$ MPa; 7·020 (7), 7·536 (7), 13·216 (10), 83·77 (8), 87·53 (8), 70·19 (8) at $9{\cdot}8\times10^2$ MPa.

	x	*y*	*z*	B_{eq}/B (Å^2)
Se(1)	2983 (3)	3358 (3)	6156 (1)	2·6
	3027 (10)	3345 (5)	6160 (3)	2·5
Se(2)	1653 (3)	7499 (3)	5112 (1)	2·4
	1620 (10)	7515 (5)	5113 (3)	2·5
Se(11)	3718 (3)	1693 (2)	3867 (1)	2·5
	3781 (10)	1648 (5)	3864 (3)	2·3
Se(12)	2297 (3)	5832 (2)	2812 (1)	2·4
	2264 (9)	5848 (5)	2788 (3)	2·2
P	0	0	0	2·8
	0	0	0	1·9
F(1)	266 (27)	−1129 (17)	1069 (9)	5·9
	289 (50)	−1140 (28)	1113 (14)	5·0
F(2)	2278 (23)	−1029 (21)	−215 (16)	7·9
	2412 (57)	−1141 (42)	−177 (25)	8·1
F(3)	444 (28)	1637 (19)	460 (12)	6·4
	563 (49)	1622 (28)	497 (16)	3·3
C(1)	2221 (35)	5364 (27)	6975 (16)	2·9
	2239 (80)	5365 (47)	6976 (24)	1·8
C(2)	1655 (26)	7111 (23)	6558 (15)	2·2
	1529 (84)	7129 (51)	6579 (26)	2·5
C(3)	2508 (28)	4919 (25)	4949 (14)	1·8
	2506 (72)	4901 (47)	4953 (24)	1·8
C(4)	971 (34)	8899 (28)	7059 (17)	3·2
	895 (81)	8957 (47)	7040 (24)	1·7
C(5)	2355 (33)	4738 (31)	8113 (17)	3·4
	2481 (90)	4616 (56)	8133 (29)	3·2
C(11)	3743 (26)	2059 (24)	2446 (13)	1·6
	3728 (78)	2035 (45)	2417 (23)	1·5
C(12)	3089 (28)	3846 (24)	1970 (13)	1·9
	3142 (83)	3772 (48)	1976 (25)	2·1
C(13)	2762 (29)	4280 (25)	4027 (14)	2·2
	2823 (80)	4280 (45)	4040 (23)	1·7
C(14)	2970 (33)	4365 (27)	881 (13)	2·5
	2897 (79)	4402 (47)	864 (24)	1·9
C(15)	4444 (31)	330 (26)	1935 (15)	2·5
	4589 (77)	287 (45)	1925 (24)	1·8

both sides of the peaks. The final number of independent reflections retained 'as observed' for the refinement was then 954 at $6{\cdot}5\times10^2$ MPa and 491 at $9{\cdot}8\times10^2$ MPa.

Both high-pressure structures were refined in the same way as for the low-temperature ones. Atomic scattering factors were from Bacon (1972, 1974). Anisotropic thermal parameters were only considered for the selenium atoms. The final reliability factors are $R=0{\cdot}048$ and $R=0{\cdot}067$ for the $6{\cdot}5\times10^2$* and 9.8×10^2 MPa structures respectively. Atomic coordinates are given in Table 2, bond lengths and angles are displayed in Fig. 4.

Thermal expansion and isothermal compressibility

The 4 to 295 K *thermal expansion* of the unit cell of a $(TMTSF)_2PF_6$ single crystal is displayed in Fig. 1. The cell parameters smoothly evolve in the whole temperature range except for a broad minimum at ~60 K in γ and a broad maximum at ~17 K in β. No anomaly is visible in the vicinity of the 'metal-insulator' phase-transition temperature ($T_{MI}=11{\cdot}5$ K). This result is in agreement with those of Guy, Marseglia, Parkin, Friend & Bechgaard (1982) and also with the *a* expansion measured with a very sensitive capacitance technique by Gaonach, Creuzet & Moradpour (1985). However, with sound-velocity measurements, Chaikin, Tiedje & Bloch (1982) have observed two anomalies in the elastic properties of $(TMTSF)_2PF_6$, namely a weak one at ~55 K (a temperature close to our 60 K) and a second one at ~12 K attributed to the 'metal-insulator' transition.

A quantitative analysis of the data in Fig. 1 leads to a^*, b^*, c^* thermal expansions (3·3, 1·6, 1·3% in the range 13 to 295 K) similar to those given by Guy *et al.* (1982), *i.e.* 3·6, 1·6 and 1·3%, respectively, in the range 10 to 300 K.

To examine the results in greater detail, we have fitted the expansion of each cell parameter with continuous functions over the whole temperature range, although we know that transitions exist at ~11·5 and 55 K and may correspond to discontinuities. This approach leads to the following results.

The volumic thermal expansion $\alpha_v=(1/v)(\partial v/\partial T)_P$ of $(TMTSF)_2PF_6$ first decreases slowly and quasi-linearly from its room-temperature value [$\alpha_v(300\text{ K})\simeq0{\cdot}27\times10^{-3}$ K^{-1}] down to ~60 K, where a progressive increase of the slope is observed. α_v thus becomes very small at low temperature and even slightly negative below ~12 K.

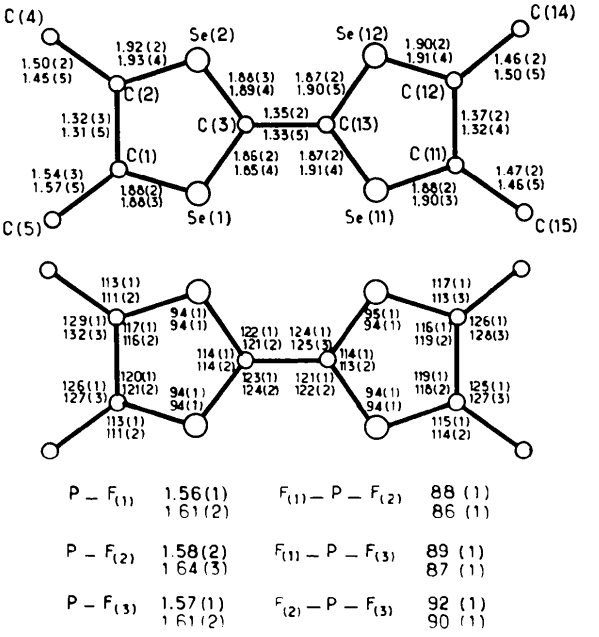

Fig. 4. Bond lengths (Å) and angles (°) for $(TMTSF)_2PF_6$ structures under $6{\cdot}5\times10^2$ MPa and $9{\cdot}8\times10^2$ MPa at room temperature. For each quantity the $9{\cdot}8\times10^2$ MPa value is displayed below the $6{\cdot}5\times10^2$ MPa one. E.s.d.'s are given in parentheses.

* See deposition footnote.

At room temperature the values of the linear expansions along the cell axes are $\alpha_a \simeq 1{\cdot}6\times10^{-4}$, $\alpha_b \simeq 0{\cdot}22\times10^{-4}$, $\alpha_c \simeq 0{\cdot}61\times10^{-4}\,K^{-1}$. When T decreases, α_a decreases rapidly, α_c remains nearly constant and α_b increases slowly. α_c and α_a become smaller than α_b at about 60 and 40 K, respectively, and both are negative in the range 10–15 K. α_b shows a broad maximum at about 40 K [$\alpha_b(40\,K) \simeq 0{\cdot}48\times10^{-4}\,K^{-1}$].

We may also note that at room temperature the expansion of $(TMTSF)_2PF_6$ along the chain axis is ~10% larger than in TTF-TCNQ at the same temperature (Filhol, Bravic, Gaultier, Chasseau & Vettier, 1981; $\alpha_b \simeq 1{\cdot}47\times10^{-4}\,K^{-1}$). The same percentage is observed down to 100 K.

The magnitudes and directions of the principal expansion coefficients [$\alpha_i = (1/l_i)(\partial l_i/\partial T)_P$] have been computed. The room-temperature values ($\alpha_1 \simeq 2{\cdot}25\times10^{-4}$, $\alpha_2 \simeq 0{\cdot}63\times10^{-4}$, $\alpha_3 \simeq -0{\cdot}19\times10^{-4}\,K^{-1}$) indicate a somewhat larger anisotropy than those published by King & La Placa (1981) ($\alpha_1 = 1{\cdot}72\times10^{-4}$, $\alpha_2 = 0{\cdot}49\times10^{-4}$, $\alpha_3 = -0{\cdot}18\times10^{-4}\,K^{-1}$). The anisotropy ratio (2·5:0·7:−0·2 at 300 K) is nearly constant down to ~140 K, has a minimum value (1·6:0·9:0·5) at ~55 K and increases rapidly at lower temperatures.

If we now consider the directions of the principal expansion coefficients (inset of Fig. 5), it is surprising that the largest expansion (α_1) is *not along the stacking direction* as in most 1D organic conductors,* but is offset by 25–40° from the a axis at all temperatures. Note that King & La Placa (1981) also found an offset value of ~30° at 300 K. A second striking point is that the α_1 direction largely precesses around the a axis. Surprisingly, the α_1's undergo pronounced displacements with temperature and do not match simple structural directions. However, at ~15 K the projections of α_2 and α_3 on the bc plane are respectively nearly normal and parallel to the long axis of the TMTSF molecules.

To understand fully the somewhat complicated thermal-expansion behaviour of $(TMTSF)_2PF_6$, more accurate data and a more detailed study are required. However, we postulate that the metal-insulator phase transition is associated with the thermal contraction below ~12 K in the crystal plane defined by the a axis and the long axis of the TMTSF molecules. The expansion data also confirm the existence at 50–60 K of a change in the structural behaviour; the following discussion gives evidence that this change is due to a 'freezing out' of the PF_6^- anion.

The *isothermal compressibility* of the $(TMTSF)_2PF_6$ unit cell has been measured up to 16×10^2 MPa. Cell parameters evolve similarly when pressure is increased (Fig. 3) as when temperature is lowered. However, we note that the effect of 16×10^2 MPa compared with that of a temperature drop from 300 to 4 K is of the same magnitude on cell angles but about twice as large on cell volume and dimensions.

The bulk modulus $B = k_v^{-1}$ and its derivative $B' = (dB/dP)$ fitted using the Murnaghan equation of state $\{P = (B/B')[(V_0/V)^{B'} - 1]\}$ are found to be $B \simeq 100\times10^2$ MPa and $B' \simeq 2$. These values, compared with those observed by Filhol *et al.* (1981) in TTF-TCNQ ($B = 114\times10^2$ MPa, $B' = 6$) indicates that $(TMTSF)_2PF_6$ is slightly more compressible than TTF-TCNQ (Fig. 6). The pressure dependence of the cell dimensions is quasi-linear in the experimental pressure range (Fig. 3) and the corresponding room-pressure linear compressibilities are $k_a = 0{\cdot}41\times10^{-4}$, $k_b = 0{\cdot}27\times10^{-4}$, $k_c = 0{\cdot}25\times10^{-4}\,MPa^{-1}$.

* For example: TTF-TCNQ (Filhol *et al.*, 1981); triethylammonium-$(TCNQ)_2$ (Filhol & Thomas, 1984). However, iodine-containing salts behave differently with a transverse expansion larger than the longitudinal one in (tetrathiotetracene)-$I_{3+\delta}$ from room temperature (Filhol, Gaultier, Hauw, Hilti & Mayer, 1982) and in trimethylammonium-TCNQ-I (Filhol, Rovira, Hauw, Gaultier, Chasseau & Dupuis, 1979) below 250 K.

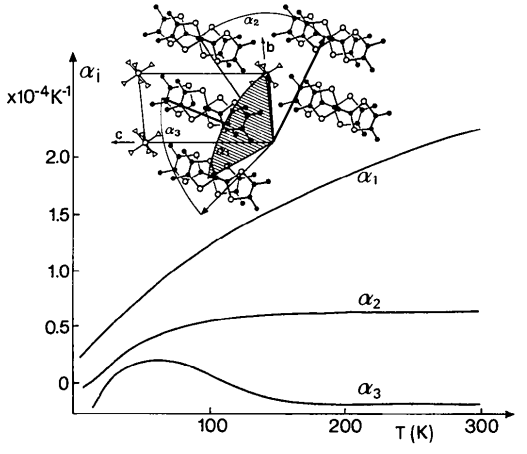

Fig. 5. Magnitudes [$\alpha_i = (1/l_i)(\partial l_i/\partial T)_P$] and directions of the principal thermal expansions in $(TMTSF)_2PF_6$. The directions are indicated in the inset by vectors of equal arbitrary modulus (thin vectors: 100 K, thick vectors: 15 K).

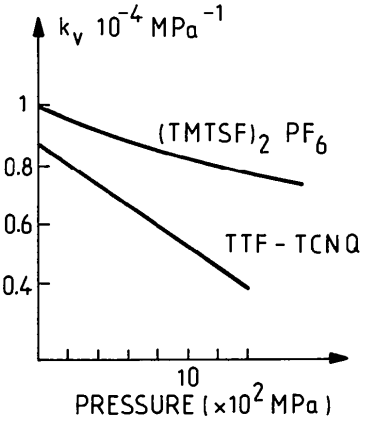

Fig. 6. Volumic compressibility [$k_v = -(1/V)(\partial V/\partial P)_T$] in $(TMTSF)_2PF_6$ and in TTF-TCNQ as a function of pressure.

The magnitudes $[k_i = -(1/l_i)(\partial l_i/\partial P)_T]$ and the directions ($\mathbf{k}_i$) of the principal compressibilities of $(TMTSF)_2PF_6$ (Fig. 7) have also been derived from data in Fig. 3. The observed anisotropy is in the ratio (1·7:0·9:0·4) under 0·1 MPa and (1·5:0·9:0·6) under 16×10^2 MPa. The largest (k_1) and intermediate (k_2) principal compressibilities show a quasi-linear increase with pressure whereas the smallest one (k_3) exhibits a flat maximum at $\sim 11 \times 10^2$ MPa.

At room temperature and under normal pressure, the directions ($\mathbf{k}_i$) of the principal compressibilities are roughly that of the principal expansions ($\boldsymbol{\alpha}_i$). Furthermore, when P increases the $\mathbf{k}_i$'s rotate in the opposite directions to that of the $\boldsymbol{\alpha}_i$'s when the temperature decreases, but with much smaller changes in their respective orientations. More precisely, the direction of the largest compressibility ($\mathbf{k}_1$) is offset by ~38° at 0·1 MPa from the chain axis and is nearly parallel to the largest thermal expansion ($\boldsymbol{\alpha}_1$) at high temperature. This offset is reduced to ~19° at 16×10^2 MPa. $\mathbf{k}_2$ and $\mathbf{k}_3$ remain close to the TMTSF molecular plane.

Structures at low temperature or under high pressure

No evidence has been found of a loss of the inversion centre under constraint and no major modification of the short intra- and interchain Se···Se and Se···F interaction network is observed. Therefore, the atom and interaction labelling used by Thorup *et al.* (1981) for the 295 K, 0·1 MPa structure is kept in the following. Before starting a more detailed comparison of the various structures we must point out that though the neutron low-temperature results are fairly precise the X-ray high-pressure ones (with fewer data) are of similar accuracy for the Se atoms but provide larger e.s.d.'s for the lighter atoms (*i.e.* C and F atoms; positions of H atoms not refined) (Figs. 2 and 4). However, this only precludes the possibility of an analysis of the effect of T or P on the intramolecular parameters.

The 4 K structure (below T_{MI}) and the 20 K structure (above T_{MI}) are reported here (Table 4, Fig. 2). They show minor structural changes at the metal-insulator phase transition and thus the following discussion mainly refers to the 4 K results only.

(i) *Intrachain interactions*

At low temperature or under high pressure the TMTSF units are nearly planar as already observed at 300 K and 0·1 MPa by Thorup *et al.* (1981). The TMTSF stacks (Fig. 8) remain of zig-zag type with only minor modifications in their geometrical parameters except for the interplanar spacing as discussed later.

More precisely, the tilt angle between the a cell axis and the normal to the TMTSF molecular plane remains almost constant (~1·1° at 295 K and

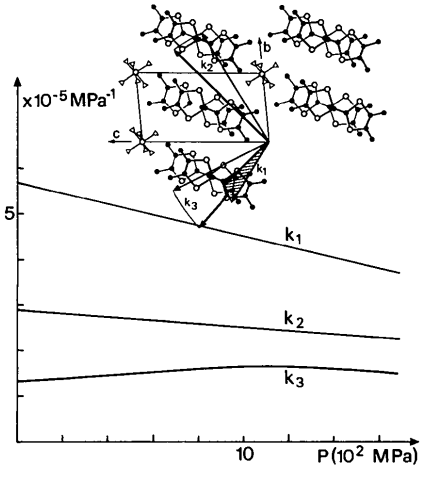

Fig. 7. Magnitude $[k_i = -(1/l_i)(\partial l_i/\partial P)_T]$ and directions of the principal isothermal compressibilities in $(TMTSF)_2PF_6$. The directions are indicated in the inset by vectors all of equal arbitary modulus (thin vectors: 0·1 MPa, thick vectors: 16×10^2 MPa).

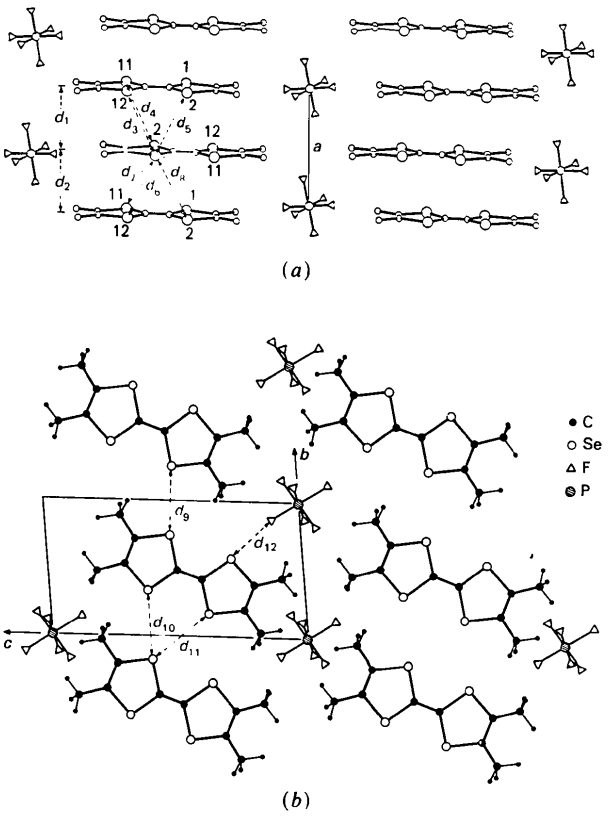

Fig. 8. The room structure of $(TMTSF)_2PF_6$. (*a*) Projection in the (a, [011]) plane. d_1 and d_2 are interplanar spacings. d_3 to d_8 are independent short intrachain Se···Se distances. (A given TMTSF molecule is involved in twelve non-independent short distances d_3 to d_8.) (*b*) Projection along cell axis a. d_9, d_{10} and d_{11} label the shortest interchain Se···Se distances and d_{12} is the shortest Se···F distance.

Table 3. *Interplanar distances (d_1 and d_2) and overlap parameters (δ_i) in TMTSF stacks*

d_1 and d_2 (in Å): distances between the mean molecular plane of an (x, y, z) TMTSF molecule and the $(1-x, 1-y, 1-z)$ or $(-x, 1-y, 1-z)$ adjacent one respectively. The mean molecular planes were calculated over atoms C(3), C(13) and Se. E.s.d.'s are given in parentheses.

δl_1 and δl_2; δt_1 and δt_2 (in Å): relative shifts of molecular centre of mass along (δl) and across (δt) the molecular elongation axis.

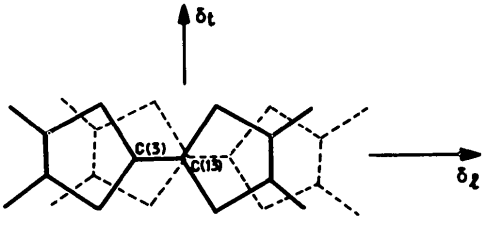

	295 K (0·1 MPa)	4 K (0·1 MPa)	$6{\cdot}5\times10^2$ MPa (295 K)	$9{\cdot}8\times10^2$ MPa (295 K)
d_1	3·664 (5)	3·55 (1)	3·56 (1)	3·50 (1)
d_2	3·630 (5)	3·52 (1)	3·56 (1)	3·50 (1)
δl_1	1·666 (2)	1·648 (2)	1·625 (6)	1·57 (1)
δt_1	0·033 (2)	0·005 (3)	0·055 (7)	0·08 (1)
δl_2	1·453 (2)	1·468 (2)	1·436 (6)	1·43 (1)
δt_2	0·052 (2)	0·064 (3)	0·064 (7)	0·09 (1)

0·1 MPa, ~1·3° at 4 K and 0·1 MPa; 1.2° at 295 K and $9{\cdot}8\times10^2$ MPa). The major change in the *overlap* of adjacent molecules within a stack is a small reduction (~0·03 Å) in the transverse shift parameter (Δt) at low temperature (Table 3). Therefore, the interplanar distances* almost fully characterize the temperature and pressure effect on the TMTSF stacks in $(TMTSF)_2PF_6$. We observe an overall quasi-linear shortening $\{[(1/d)\Delta d/\Delta T]_P \simeq 1{\cdot}0\times10^{-4}\,K^{-1}$ and $[-(1/d)\Delta d/\Delta P]_T \simeq 0{\cdot}42\times10^{-4}\,MPa^{-1}\}$ in the experimental temperature and pressure range respectively.

This effect is fully accounted for by the a contraction of the unit cell since the angle between the a axis and the TMTSF molecular plane is constant. Similar behaviour has been observed in TTF-TCNQ stacks (Filhol *et al.*, 1981) with comparable magnitudes ($\sim0{\cdot}8\times10^{-4}\,K^{-1}$, $\sim0{\cdot}41\times10^{-4}\,MPa^{-1}$ respectively), even though there are Se···Se intrastack interactions in the former compound and much weaker N···N and S···S interactions in the latter.

The major difference between the temperature and the pressure effects seems to be in the relative behaviour of the two independent intrastack interplanar distances d_1 and d_2 (see Fig. 8). If the difference $\Delta = |d_1 - d_2|$ is taken as the criterion for the diadic character of the columns, this character is weak under normal conditions (0·03 Å at 295 K, 0·1 MPa), unchanged down to 4 K but vanishes in the $6{\cdot}5\times10^2$ and $9{\cdot}8\times10^2$ MPa structures (Table 4).

* The mean plane is defined by the C(3), C(13) and Se atoms.

Table 4. *Short* Se···Se *and* Se···F *distances* (Å) *labelled in Fig.* 8

E.s.d.'s are given in parentheses.

	T, 0·1 MPa			295 K, *P*	
	300 K*	20 K	4 K	$6{\cdot}5\times10^2$ MPa	$9{\cdot}8\times10^2$ MPa
Intrastack distances					
d_1	3·66	3·54 (1)	3·55 (1)	3·56 (1)	3·50 (1)
d_2	3·63	3·52 (1)	3·52 (1)	3·56 (1)	3·50 (1)
d_3	4·044 (2)	3·906 (7)	3·915 (7)	3·958 (3)	3·885 (6)
d_4	3·983 (2)	3·857 (7)	3·861 (7)	3·891 (3)	3·810 (6)
d_5	4·067 (2)	3·945 (7)	3·943 (7)	3·979 (3)	3·924 (6)
d_6	3·874 (2)	3·857 (7)	3·866 (7)	3·817 (3)	3·780 (6)
d_7	3·927 (2)	3·800 (7)	3·799 (7)	3·872 (3)	3·834 (6)
d_8	4·133 (2)	4·052 (7)	4·054 (7)	4·061 (3)	3·995 (6)
Interstack distances					
d_9	3·879 (1)	3·707 (7)	3·711 (7)	3·732 (3)	3·657 (6)
d_{10}	3·934 (1)	3·741 (7)	3·737 (7)	3·777 (3)	3·678 (6)
d_{11}	3·959 (2)	3·859 (7)	3·857 (7)	3·847 (3)	3·753 (6)
Shortest Se···F distance					
d_{12}	3·233 (7)	3·068 (9)	3·060 (9)	3·123 (13)	3·005 (23)

* Thorup *et al.* (1981).

Finally, we note that a plot of the intrastack Se···Se distances labelled in Fig. 8 *versus* pressure (Fig. 9) indicates an equivalent shortening for, say, a cooling to 4 K or an applied pressure of 8×10^2 MPa from the normal conditions.

(ii) *Interchain interactions*

As is apparent from the thermal expansion and isothermal compressibility study of $(TMTSF)_2PF_6$, the interchain coupling is increased at low temperature or under high pressure. The Se···Se interchain interactions in particular show a quasi-linear shortening $[(1/d)\Delta d/\Delta T \simeq 1{\cdot}4\times10^{-4}\,K^{-1}$; $-(1/d)\Delta d/\Delta P \simeq 0{\cdot}60\times10^{-4}\,MPa^{-1}]$ in the experimental temperature or pressure range, respectively. In both cases the intrachain *versus* the interchain

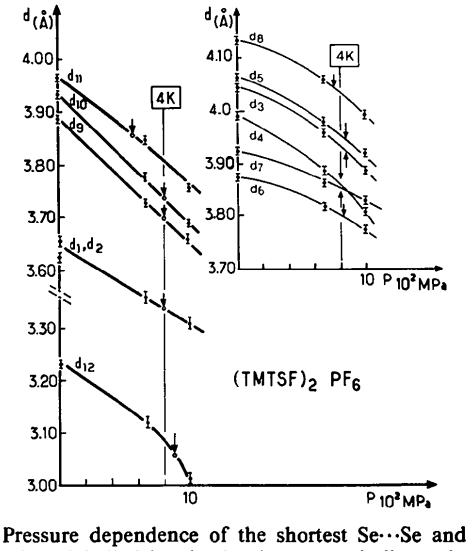

Fig. 9. Pressure dependence of the shortest Se···Se and Se···F interactions labelled in Fig. 8. The arrows indicate the corresponding values observed at 4 K under normal pressure.

Table 5. *Observed values of the φ angles (°) (see Fig. 10) between a TMTSF molecular plane and the directions of the shortest* Se···Se *distances (Å) to the nearest TMTSF molecules, which are given below the corresponding φ angles*

E.s.d.'s are given in parentheses.

	295 K (0·1 MPa)	4 K (0·1 MPa)	$6{\cdot}5\times10^2$ MPa (295 K)	$9{\cdot}8\times10^2$ MPa (295 K)
φ_1	18·44 (3)	15·99 (13)	17·73 (5)	16·42 (15)
	3·879 (1)	3·711 (6)	3·732 (3)	3·651 (5)
φ_2	18·24 (3)	14·97 (12)	16·57 (5)	15·57 (15)
	3·934 (1)	3·737 (6)	3·777 (1)	3·678 (5)
φ_3	35·73 (3)	38·02 (12)	36·90 (5)	38·10 (15)
	4·167 (2)	4·156 (7)	4·097 (3)	4·156 (8)
φ_4	54·89 (3)	53·41 (10)	54·75 (4)	54·32 (12)
	5·941 (2)	5·620 (6)	5·721 (3)	5·545 (8)

shortenings of the Se···Se distances are in the ratio 1:1·5 (Table 4). Since the mean direction of the Se···Se interchain interactions is along **b**, this clearly indicates an increase in the two-dimensional character of TMTSF coupling in $(TMTSF)_2PF_6$. A similar observation has already been made by Beno, Williams, Lee & Cowan (1982) from the 295 and 125 K structures of $(TMTSF)_2AsF_6$.

In the $(TMTSF)_2X$ salts, as well as in the isostructural sulfur analogues $(TMTTF)_2X$, the crystal packing is characterized by (a, b) sheets of TMTSF (or TMTTF) chains coupled in the **b** direction *via* strong Se···Se (or S···S) interactions. Therefore, one of the key parameters in the understanding of the electrical behaviour of these materials is the strength of the interchain coupling and more precisely the nature of the transverse orbital overlap in the *ab* plane. Grant (1985) and Yamaji (1983) have stressed that the most pertinent structural parameters here are a set of φ_i angles (Fig. 10) between the TMTSF molecular plane and the shortest Se···Se interactions with the nearest TMTSF molecules. Yamaji (1983) has suggested that

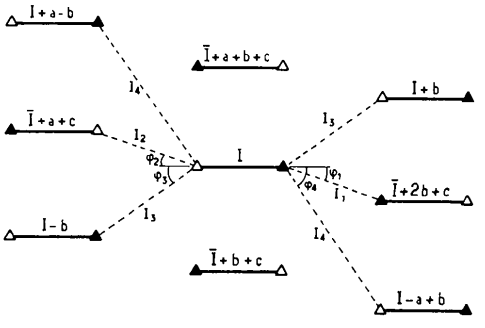

Fig. 10. Definition of the φ_i angles. The picture is a schematic representation of the TMTSF packing in the *ab* plane. Black and white triangles indicate Se(2) and Se(11) atoms respectively. The translation operation from the central TMTSF unit (labelled I) to the other units is indicated. The observed values of the φ_i angles are listed in Table 5 together with the corresponding shortest Se···Se distances.

Table 6. *Relative shift (Δ) under constraint of TMTSF molecules in the ab plane*

Δ is the displacement of a given TMTSF molecule from its position under normal conditions towards molecule I (see Fig. 10). The directions of the x, y, z components of Δ are defined in the inset figure with respect to molecule I. All values are in Å. E.s.d.'s are $<0{\cdot}01$ Å.

Molecule I

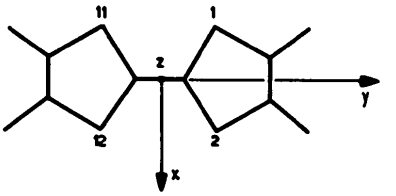

TMTSF molecule	4 K (0·1 MPa)	$6{\cdot}5\times10^2$ MPa (295 K)	$9{\cdot}8\times10^2$ MPa (295 K)
$\bar{I}+2b+c$	$\Delta x=-0{\cdot}12$	$\Delta x=-0{\cdot}17$	$\Delta x=-0{\cdot}08$
	$\Delta y=-0{\cdot}04$	$\Delta y=-0{\cdot}03$	$\Delta y=-0{\cdot}04$
	$\Delta z=-0{\cdot}19$	$\Delta z=-0{\cdot}21$	$\Delta z=-0{\cdot}20$
$\bar{I}+a+c$	$\Delta x=0{\cdot}07$	$\Delta x=0{\cdot}11$	$\Delta x=0{\cdot}22$
	$\Delta y=0{\cdot}06$	$\Delta y=0{\cdot}07$	$\Delta y=0{\cdot}00$
	$\Delta z=0{\cdot}28$	$\Delta z=0{\cdot}13$	$\Delta z=0{\cdot}25$

one would expect an *increase* in the transverse transfer integrals t_b under pressure due to an *increase* in angles φ_1 and φ_2. In fact we observe an overall tendency of the φ angles to *decrease* with decreasing temperature as well as under increasing pressure (Table 5). The only exception is for φ_3 whose variation is clearly related to the behaviour of the cell angle γ. The largest decrease from normal conditions is for φ_2 ($\Delta\varphi_2\simeq-3{\cdot}2°$ at 4 K; $\Delta\varphi_2\simeq-2{\cdot}7°$ at $9{\cdot}8\times10^2$ MPa). This overall behaviour is confirmed by a recent determination of the $(TMTSF)_2PF_6$ structure at 1·6 K *and* 7×10^2 MPa (Gallois, Gaultier, Filhol & Vettier, 1986) giving $\Delta\varphi_2\simeq-3{\cdot}7°$.

As far as the angle between the normal to the TMTSF molecular plane and the *a* axis may be regarded as constant, the observed variation of the $\Delta\varphi$'s may be explained through relative shifts of the TMTSF units. The shift components (x and y: respectively orthogonal to and along the elongation axis of the TMTSF molecules; z: normal to the molecular plane) are given in Table 6. For example, if we consider the $\bar{I}+2b+c$ TMTSF unit (see Fig. 10), a negative x displacement corresponds to a slip towards the space between the I and $\bar{I}+b+c$ units and thus to an *increase* in φ_1 (*idem* with $\bar{I}-a+c$ for φ_2). In contrast, a negative z displacement moves the $\bar{I}+2b+c$ molecular plane towards the I plane and thus *decreases* φ_1. The effect on φ_2 is the opposite of that on φ_1. In fact, we observe (Table 5) *larger* negative $\Delta\varphi_1$ and $\Delta\varphi_2$ values at low temperature than under high pressure since in both cases the z shift is large, the y shift is negligible and the x shift is large in the high-pressure case only (Table 6).

(iii) *Anion disorder*

As shown below, an important result concerning the behaviour of the PF_6^- anions under constraint may be established from the analysis of the thermal parameter (B_{eq}*/B) of fluorine atoms (Table 7).

In the following the F(B_{eq}) thermal parameters are compared with the corresponding average $\overline{Se}(B_{eq})$ thermal parameter under the same experimental conditions. At 295 K, 0·1 MPa the F(1)/$\overline{Se}$ and F(2)/$\overline{Se}$ ratios of the thermal parameters are large, presumably because of a dynamical positional disorder of the anion. Under high pressure the F(2)/$\overline{Se}$ ratio remains nearly constant whereas $\overline{F(1)F(3)}/\overline{Se}$ strongly decreases. Thus the pressure effect on the PF_6^- anion is a reduction of its disorder mainly in the transverse plane.

The low-temperature data (neutron diffraction) provides *nuclear* thermal parameters instead of electron cloud ones for the high-pressure (X-ray diffraction) structures. Hence a direct comparison of thermal parameters is not possible, while the F/$\overline{Se}$ criterion still holds. At 4 K the $\overline{F(1)F(3)}/\overline{Se}$ ratio is close to one and F(2)/$\overline{Se}$ is 1·36. At low temperature the anion disorder is thus almost completely suppressed.

Furthermore, only unique fluorine positions are observed on nuclear density maps at 4 K in contrast with $(TMTSF)_2X$ salts with non-centrosymmetric anions which show an anion twofold disorder at room temperature (order–disorder phase transition). In addition, we found no evidence of a superstructure in $(TMTSF)_2PF_6$ at 4 K despite the use of a large counting time. This strongly supports the assumption that the PF_6^- degrees of freedom are progessively reduced under constraint with an almost complete freezing at low temperature without change in the lattice symmetry. If the superstructure nevertheless exists, it will thus correspond to very small atomic displacements.

* $B_{eq} = \frac{1}{3}\sum_i \sum_j \beta_{ij} \mathbf{a}_i.\mathbf{a}_j$.

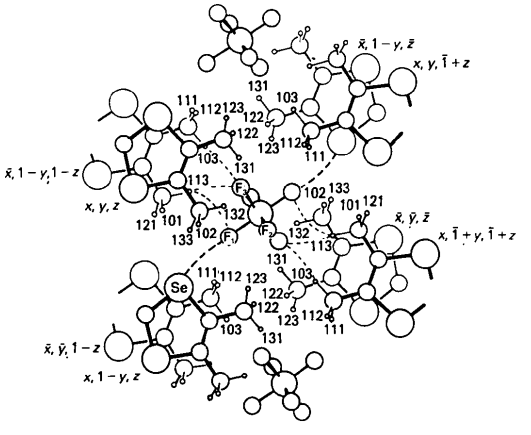

Fig. 11. Molecular environment of a PF_6^- anion. The picture is a projection along **a** of the 4 K neutron structure. The heavy dashed lines indicate the shortest Se···F distances between cations and anions while light ones indicate the shortest CH_2–H···F distances.

Table 7. *Comparison of the equivalent isotropic thermal parameter* B_{eq} (Å^2) *of* F *atoms and the average* B_{eq} *value of* Se *atoms*

	295 K 0·1 MPa	295 K $6{\cdot}5\times10^2$ MPa	295 K $9{\cdot}8\times10^2$ MPa	4 K 0·1 MPa
F(1)	8·75	5·90	5·00	0·50
F(2)	11·12	7·90	8·10	0·71
F(3)	9·36	6·40	3·30	0·57
$\overline{Se}$	2·84	2·50	2·37	0·52
P	3·68	2·80	1·90	0·20*
F(2)/$\overline{F(1)(F3)}$	1·23	1·28	1·92	1·32
F(2)/$\overline{Se}$	3·91	3·16	3·37	1·36
$\overline{F(1)F(3)}/\overline{Se}$	3·18	2·46	1·75	1·02

* The refinement of this thermal parameter gave odd results and thus the value given here is only indicative.

The interactions between TMTSF stacks and anions (Fig. 11) are enhanced under constraint and become significant with a short Se–F(1) distance [d_{12} = 3·060 (9) Å at 4 K, d_{12} = 3·00 (2) Å under $9{\cdot}8\times10^2$ MPa] compared with the sum of the atomic van der Waals radii ($r_{Se}+r_F$ = 3·35 Å). Low-temperature neutron structures in which the H atoms were precisely located show a second type of short distance, namely a set of F···H–CH_2 bonds (Fig. 11) between the TMTSF methyl groups surrounding a PF_6^- anion.

The shortest distances [F(3)···HC(5), F(3)···HC(4)] are characteristic of weak H bonds with H···F distances (2·45, 2·46 Å respectively at 4 K) less than the sum of atomic van der Waals radii (r_F+r_H = 2·52 Å) and have appropriate bond angles F···H–C (156, 140° respectively). A third short distance [F(1)···HC(4) ≃ 2·56 Å] may also be noted.

It is now striking that all the observed Se···F and H···F interactions between TMTSF cations and PF_6^- anions are close to the transverse *bc* plane and concern the fluorine atoms [F(1) and F(3)] whose thermal-motion amplitude is the most reduced by the T or P constraints. This observation relative to $(TMTSF)_2PF_6$ is similar to that made by Beno, Blackman, Leung & Williams (1983) on another Bechgaard salt with a centrosymmetric anion, namely $(TMTSF)_2AsF_6$. At 125 K the latter compound also shows Se···F cation–anion interactions and H···F ones, which are, however, all larger than 2·5 Å at that temperature.

(iv) *Comparison with* $(TMTSF)_2ClO_4$

This comparison is of special interest since $(TMTSF)_2ClO_4$ is the only Bechgaard salt which exhibits a superconducting ground state at normal pressure ($T_{s.c.}$ ≃ 1·2 K)(Bechgaard, Carneiro, Olsen, Rasmussen & Jacobsen, 1981). It also presents an anion order–disorder phase transition at ~24 K with a cell doubling (a, $2b$, c). Both the room-temperature

Table 8. *Comparison between selected structural data for* $(TMTSF)_2ClO_4$ *and* $(TMTSF)_2PF_6$

The interplanar distances (d_1 and d_2), the short Se···Se interchain distances (d_9, d_{10}, d_{11}) as well as the short cation-anion interaction (d_{12}) are defined in Fig. 8. The angles φ_1 and φ_2 are defined in Fig. 10.

			Se···Se (Å)			Se···O/F (Å)		
	d_1 (Å)	d_2 (Å)	d_9	d_{10}	d_{11}	d_{12}	φ_1 (°)	φ_2(°)
$(TMTSF)_2ClO_4$								
300 K[a]	3·64	3·63	3·778	3·865	3·955	3·34	17·1	16·3
10 K[b]	3·56	3·52	3·56	3·72	3·79	3·35 3·49	13·9	12·1
$(TMTSF)_2PF_6$								
300 K[c]	3·66	3·63	3·879	3·934	3·959	3·233	18·4	18·2
4 K	3·55	3·52	3·711	3·737	3·857	3·060	16·0	15·0
$6·5\times10^2$ MPa	3·56	3·56	3·732	3·777	3·847	3·12	17·7	16·6
$9·8\times10^2$ MPa	3·50	3·50	3·657	3·678	3·753	3·00	16·4	15·6

References: (*a*) Rindorf *et al.* (1982); (*b*) Gallois *et al.* (1985); (*c*) Thorup *et al.* (1981).

structure (Rindorf, Soling & Thorup, 1982) and the 10 K structure in the ordered ground state (Gallois *et al.*, 1985) are known. Selected data relative to this compound are displayed in Table 8.

Under *normal conditions*, TMTSF interplanar distances are similar in the two compounds while the Se···Se interchain interactions d_9 and d_{10} are shorter by ~0·10 and 0·07 Å respectively in the ClO_4^- salt than in the PF_6^- one. In addition, the anion-cation coupling appears to be weaker (Se···O ≃ 3·34 Å) in the former compound than in the latter (Se···F ≃ 3·23 Å) since the sum of the van der Waals atomic radii is nearly the same for both kinds of interactions.

We now compare briefly the structural behaviour of $(TMTSF)_2PF_6$ and $(TMTSF)_2ClO_4$.

Intrachain interactions. We observe that interplanar distances are similar in the two compounds both at room temperature and at low temperature.

Interchain interactions. In the PF_6^- salt at 4 K or under high pressure the d_{10} and d_{11} Se···Se distances are similar to that in the ClO_4^- salt at 10 K. In contrast, the short d_9 Se···Se distance is much larger than in the ClO_4^- salt at 10 K and only slightly shorter than in the latter compound at 300 K.

φ_1 and φ_2 angles. In $(TMTSF)_2PF_6$ at 4 K or under high pressure both angles have values slightly smaller than the observed ones in $(TMTSF)_2ClO_4$ at room temperature but much larger than in the latter salt at 10 K. Since we have established here that pressure and temperature constraints have similar effects on the $(TMTSF)_2PF_6$ packing, we may now postulate the following: (1) the values of the φ_1, φ_2 and d_9 and d_{10} interchain parameters observed in $(TMTSF)_2ClO_4$ at 10 K will be reached in $(TMTSF)_2PF_6$ at low temperatures *and* high pressures; (2) these parameters are relevant to the interpretation of the electrical behaviour of these materials. On this basis a quantum-chemical approach to the problem is in progress which makes use of the room- and low-temperature data at present available on TMTSF and TMTTF salts (Abderrabba, Ducasse & Gallois, 1985). However, to emphasize the limits of this simple picture we must note that high pressure alone up to $20–30\times10^2$ MPa will probably also result in similar structural effects.

Anion–cation coupling. Under high pressure as well as at low temperature the PF_6^- salt exhibits a strong increase in cation-anion coupling (Se···F distances shortened by ~0·20 Å) while in the perchlorate salt the Se···O interaction remains almost unchanged down to low temperatures.

To improve this structural analysis of the $(TMTSF)_2PF_6$ salt we will soon report its neutron structure at 1·7 K *and* 7×10^2 MPa. X-ray measurements at room temperature *and* under $\sim20\times10^2$ MPa are in progress.

The authors are much indebted to H. Ahsbahs (Marburg University, Federal Republic of Germany) for helpful discussions on the X-ray high-pressure technique; to K. Bechgaard (Copenhagen, Denmark) who kindly supplied the samples and to S. A. Mason (ILL, Grenoble, France) who checked the English of the manuscript.

References

ABDERRABBA, A., DUCASSE, L. & GALLOIS, B. (1985). *J. Phys. C*, **18**, L947-L951.
AHSBAHS, H. (1984). *Rev. Phys. Appl.* **19**, 819-821.
BACON, G. E. (1972). *Acta Cryst.* A**28**, 357-358.
BACON, G. E. (1974). *Acta Cryst.* A**30**, 847.
BECHGAARD, K., CARNEIRO, K., OLSEN, M., RASMUSSEN, F. B. & JACOBSEN, C. S. (1981). *Phys. Rev. Lett.* **46**, 852-855.
BECHGAARD, K., JACOBSEN, C. S., MORTENSEN, K., PEDERSEN, H. J. & THORUP, N. (1980). *Solid State Commun.* **33**, 1119-1125.
BENO, M. A., BLACKMAN, G. S., LEUNG, P. C. W. & WILLIAMS, J. M. (1983). *Solid State Commun.* **48**, 99-103.
BENO, M. A., WILLIAMS, J. M., LEE, M. M. & COWAN, D. O. (1982). *Solid State Commun.* **44**, 1195-1198.
BRIDGMANN, P. W. (1911). *Proc. Am. Acad. Arts Sci.* **47**, 441-445.
CHAIKIN, P. M., TIEDJE, T. & BLOCH, A. N. (1982). *Solid State Commun.* **41**, 739-742.
DAVIES, H. W. (1968). *J. Res. Natl Bur. Stand. Sect. A*, **72**, 149-153.
EMGE, T. J., WILLIAMS, J. M., LEUNG, P. C. W., SCHULTZ, A. J., BENO, M. A. & WANG, H. H. (1985). *Mol. Cryst. Liq. Cryst.* **119**, 237-240.

FILHOL, A., BRAVIC, G., GAULTIER, J., CHASSEAU, D. & VETTIER, C. (1981). *Acta Cryst.* B37, 1225-1235.

FILHOL, A., GAULTIER, J., HAUW, C., HILTI, B. & MAYER, C. W. (1982). *Acta Cryst.* B38, 2577-2589.

FILHOL, A., ROVIRA, M., HAUW, C., GAULTIER, J., CHASSEAU, D. & DUPUIS, P. (1979). *Acta Cryst.* B35, 1652-1660.

FILHOL, A. & THOMAS, M. (1984). *Acta Cryst.* B40, 44-59.

FINGER, L. W., BENO, M. A., WILLIAMS, J. M. & HAZEN, R. M. (1984). *Acta Cryst.* A40, C150.

GALLOIS, B., CHASSEAU, D., GAULTIER, J., HAUW, C., FILHOL, A. & BECHGAARD, K. (1983). *J. Phys. (Paris) Colloq.* 44, 1071-1074.

GALLOIS, B., GAULTIER, J., FILHOL, A. & VETTIER, C. (1986). In preparation.

GALLOIS, B., MERESSE, A., GAULTIER, J. & MORET, R. (1985). *Mol. Cryst. Liq. Cryst.* 131, 147-161.

GAONACH, C., CREUZET, G. & MORADPOUR, A. (1985). *Mol. Cryst. Liq. Cryst.* 119, 265-268.

GRANT, P. M. (1985). *Proc. of the International Conference on the Physics and Chemistry of Low Dimensional Synthetic Metals, Abano Terme, Italy.*

GUY, D. R. P., MARSEGLIA, E. A., PARKIN, S. S. P., FRIEND, R. H. & BECHGAARD, K. (1982). *Mol. Cryst. Liq. Cryst.* 79, 337-341.

International Tables for X-ray Crystallography (1974). Vol. IV. Birmingham: Kynoch Press. (Present distributor D. Reidel, Dordrecht.)

JÉROME, D., MAZAUD, A., RIBAULT, M. & BECHGAARD, K. (1980). *J. Phys. (Paris) Lett.* 41, L95-L98.

JÉROME, D. & SCHULZ, H. J. (1982). *Adv. Phys.* 31, 299-490.

KING, H. E. & LA PLACA, S. J. (1981). *Bull. Am. Phys. Soc.* 26, 214.

LEHMANN, M. S. & LARSEN, F. K. (1974). *Acta Cryst.* A30, 580-584.

LOUMRHARI, H. (1983). Thesis No. 1864, Univ. de Bordeaux I.

MORET, R., POUGET, J. P., COMÈS, R. & BECHGAARD, K. (1982). *Phys. Rev. Lett.* 49, 1008-1012.

RINDORF, G., SOLING, H. & THORUP, N. (1982). *Acta Cryst.* B38, 2805-2808.

RINDORF, G., SOLING, H. & THORUP, N. (1984). *Acta Cryst.* C40, 1137-1139.

THORUP, N., RINDORF, G., SOLING, H. & BECHGAARD, K. (1981). *Acta Cryst.* B37, 1236-1240.

TORRANCE, J. B., PEDERSEN, H. J. & BECHGAARD, K. (1982). *Phys. Rev. Lett.* 49, 881-884.

YAMAJI, K. (1983). *Proceedings of the* 6th *Taniguchi Symposium on Magnetic Superconductors and Their Related Problems, Kashikojima, Japan.* Berlin: Springer Verlag.

ZEYEN, C. M. E., CHAGNON, R., DISDIER, F. & MORIN, H. (1984). *Rev. Phys. Appl.* 19, 789-791.

Acta Cryst. (1986). B42, 575-601

Propellanes LXXIX.* Comparison of the Geometries of Dithia[*n*.3.3]propellanes ($n = 1, 2, 3$) and Dithia(and Oxathia)[4.3.3]propellenes. Study of the Influence of Complexation with $HgCl_2$, I_2, $CdCl_2$ and $PdCl_2$ and of Formation of Sulfoxides on some of these Compounds. Demonstration of the 'Klammer' Effect. Structures of Eighteen Crystals

BY FRANK H. HERBSTEIN, PNINA ASHKENAZI, MENAHEM KAFTORY, MOSHE KAPON, GEORGE M. REISNER AND DAVID GINSBURG

Department of Chemistry, Technion-Israel Institute of Technology, Haifa, Israel 32000

(*Received* 17 *July* 1985; *accepted* 23 *April* 1986)

Abstract

The room-temperature crystal structures of eighteen compounds are reported. There are twelve molecular structures: dithia[3.3.1]propellane [$C_7H_{10}S_2$, *Cc*, $a = 6{\cdot}626\ (3)$, $b = 41{\cdot}077\ (20)$, $c = 6{\cdot}600\ (3)$ Å, $\beta = 120{\cdot}11\ (5)°$, $Z = 8$, $R_F = 0{\cdot}057$ for 1164 reflections], dithia[3.3.3]propellane [$C_9H_{14}S_2$, $P2_1/n$, $a = 11{\cdot}462\ (5)$, $b = 11{\cdot}428\ (5)$, $c = 7{\cdot}313\ (4)$ Å, $\beta = 95{\cdot}68\ (5)°$, $Z = 4$, $R_F = 0{\cdot}069$ for 1363 reflections] and dithia[4.3.3]propellene [$C_{10}H_{14}S_2$, $P2_1/c$, $a = 6{\cdot}897\ (4)$, $b = 23{\cdot}063\ (11)$, $c = 12{\cdot}656\ (6)$ Å, $\beta = 91{\cdot}29\ (5)°$, $Z = 8$, $R_F = 0{\cdot}069$ for 2043 reflections]; the isostructural centrosymmetric dimers of dithia[3.3.3]-propellane.$HgCl_2$ [$C_9H_{14}S_2.HgCl_2$, $P2_1/c$, $a = 14{\cdot}320\ (6)$, $b = 9{\cdot}762\ (4)$, $c = 9{\cdot}058\ (4)$ Å, $\beta = 90{\cdot}32\ (5)°$, $Z = 4$, $R_F = 0{\cdot}081$ for 1927 reflections] and oxathia[4.3.3]propellene.$HgCl_2$ [$C_{10}H_{14}OS.HgCl_2$, $P2_1/c$, $a = 14{\cdot}926\ (6)$, $b = 9{\cdot}417\ (4)$, $c = 8{\cdot}744\ (4)$ Å, $\beta = 94{\cdot}77\ (5)°$, $Z = 4$, $R_F = 0{\cdot}065$ for 1907 reflections]; dithia[3.3.1]propellane.$2I_2$ [$C_7H_{10}S_2.2I_2$, $P\bar{1}$, $a = 11{\cdot}708\ (4)$, $b = 9{\cdot}491\ (3)$, $c = 7{\cdot}887\ (3)$ Å, $\alpha = 66{\cdot}03\ (5)$, $\beta = 104{\cdot}48\ (5)$, $\gamma = 110{\cdot}45\ (5)°$, $Z = 2$, $R_F = 0{\cdot}064$ for 2337 reflections] and dithia[3.3.2]-propellane.$2I_2$ [$C_8H_{12}S_2.2I_2$, $P2_1/c$, $a = 8{\cdot}428\ (3)$, $b = 21{\cdot}839\ (7)$, $c = 9{\cdot}548\ (3)$ Å, $\beta = 115{\cdot}51\ (5)°$, $Z = 4$, $R_F = 0{\cdot}042$ for 2451 reflections]; dithia[3.3.3]-propellane.$PdCl_2$ [$C_9H_{14}S_2.PdCl_2$, *Pmna*, $a = 13{\cdot}515\ (5)$, $b = 7{\cdot}412\ (4)$, $c = 11{\cdot}801\ (5)$ Å, $Z = 4$, $R_F = 0{\cdot}045$ for 1025 reflections]; dithia[4.3.3]-propellene.$PdCl_2$ [$C_{10}H_{14}S_2.PdCl_2$, *Pnma*, $a = 14{\cdot}362\ (5)$, $b = 7{\cdot}422\ (4)$, $c = 11{\cdot}891\ (5)$ Å, $Z = 4$, $R_F = 0{\cdot}042$ for 994 reflections]; bis{oxathia[4.3.3]-propellene}.$PdCl_2$ [$2C_{10}H_{14}OS.PdCl_2$, *Pbca*, $a =$

* Part LXXVIII: Weinberg, Knowles & Ginsburg (1985).

0108-7681/86/060575-27$01.50